Development of a Diagnostic Damköhler Number for Interpreting Laser-Induced Fluorescence Data in Turbulent Flames

Kaylyn Beseler[1], Ankit Tyagi[2], and Jacqueline O'Connor[3]
Pennsylvania State University, University Park, PA, 16802, USA

Back-support pilot flames are commonly used for stabilization of turbulent, premixed flames in laboratory experiments. These pilot flames produce an adiabatic or super-adiabatic boundary to provide more favorable conditions for combustion. While the use of pilot flames is very common, it's unclear how these pilot flames change the structure and behavior of the turbulent flames they stabilized. In our recent study of back-support pilot flame effects on flame structure and dynamics in interacting Bunsen flames, we found that the interpretation of laser-induced fluorescence diagnostics was not straightforward in highly strained back-supported flames. In particular, the extinction behavior of these flames is significantly different than in non-back-supported flames and very high rates of steady strain do not lead to extinction as would be the case without back-support. The goal of this study is to use a combination of experiment and simulation to understand the behavior of highly-strained back-supported flames and the interpretation of laser diagnostics under these conditions. In particular, we propose a "diagnostic Damköhler number" as a metric by which one can determine if a steady laminar flamelet concept is a realistic model for interpreting laser-induced fluorescence measurements.

I. Nomenclature

Da	=	Damköhler number
K_{bulk}	=	bulk strain
S_{ij}	=	strain rate
S_L	=	laminar flame speed
T	=	temperature
Q	=	heat release rate
U	=	bulk flow velocity
$\bar{c}$	=	time-averaged progress variable
d	=	distance between nozzle exits
ℓ	=	integral length scale
ℓ_F	=	laminar flame thickness
u'	=	turbulence intensity
v	=	velocity of the jets at the nozzle exit
δ_f	=	flame thickness

II. Introduction

Turbulent combustion is a widely studied field with many different applications. Research in the turbulent combustion community benefits many practical systems with applications for vehicle engines, power generation, and aircraft engines. While turbulent combustion is ubiquitous in these power and propulsion technologies, there are still

[1] Graduate Student, Mechanical Engineering
[2] Graduate Research Assistant, Mechanical Engineering, AIAA Student Member
[3] Associate Professor, Mechanical Engineering, AIAA Senior Member

several important research questions to answer regarding the structure and dynamics of turbulent flames. In particular, the scales at which turbulence interacts with the flame and the impact that this interaction has on the flame structure and chemical pathways in the flame are areas of active research. Traditionally, the Borghi-Peters diagram is used to explain the interaction between changes in the turbulence intensity and the flame structure. The Borghi-Peters diagram identifies regimes based on the turbulence intensity (u'), the laminar flame speed (S_L), integral length scale (ℓ), and the laminar flame thickness (ℓ_F) [1]. The five flame structure regimes identified on the Borghi-Peters diagram are: laminar flames, wrinkled flamelets, corrugated flamelets, thin reaction zones, and broken reactions zones. This work considers flames in the thin reaction zone and broken reaction zone.

Much of turbulent combustion research is done on laboratory-scale flames to study fundamental turbulence-flame coupling processes. Many of these laboratory configurations often use back-support pilot flames to stabilize the flame by creating a boundary of adiabatic or super-adiabatic products around the premixed reactants that significantly reduces heat loss from the flame. Many previous turbulent combustion experiments [2]–[6] and simulations [7] have used back-support pilot flames. Previous studies with back-support pilot flames have shown that the adiabatic boundary allows for highly strained, connected flamelets to exist beyond what is predicted by the Borghi-Peters diagram. For example, turbulent Bunsen flames in the Hi-Pilot burner experiment with back-support pilot flames [8] were exposed to very high levels of relatively large length-scale turbulence – $u'/S_L \sim O(100)$ and $l/\delta_f \sim O(100)$ – and became wrinkled but did not experience extinction or even significant disconnectedness. According to the Borghi-Peters diagram, the flames should have been disturbed, leading to disconnected flames or flame extinction.

Not only does the high turbulence intensity affect the structure of the flame, it also affects the chemical pathways of the reactions occurring. In a study by Dasgupta *et al.* [9], chemical pathways in turbulent premixed methane-air flames were studied over a range of turbulence intensities. They found that changes in different parameters had different effects on dominant reactions. For example, a dominant heat release reaction ($CO + OH \rightarrow H + CO_2$) decreased around 9% as the turbulence increased. A more significant decrease of about 27% occurred as the flame stretch increased and as the residence time decreased the reaction rate decreased about 18%. Additionally, the authors looked at the production and consumption of key species in dominant reactions. In all cases, they found that the reaction rates changed as the turbulence intensity and stretch was varied. Of particular interest is the result for the production and consumption of OH; increasing the stretch changed the dominant reaction involved with the consumption and production of OH. A pool of OH radicals was formed at increased stretch due to an increase in the chain branching reactions in comparison to the chain termination reactions.

A second configuration used in turbulent flame experiments are counterflow flames. Counterflow premixed flames were found to be similar in structure to turbulent premixed jet flames by Coppola *et al.* [10]. Previous turbulent combustion experiments [11]–[13] and simulations [9], [14] have used the counter-flow flame confirmation. Certain turbulent counterflow flame experiments and simulations have been devised that mimic the effect of the back-support pilot on turbulent flames. Back-support pilot flames produce a layer of hot products parallel to the flow of the premixed reactants. These parallel flows mix across a diffusion layer and that diffusion layer mixing can be modeled using asymmetric counterflow jets. In the asymmetric counterflow configuration, one jet is composed of hot products and the opposite jet is composed of reactants. At the stagnation plane of the two jets, the products and reactants mix across the diffusion layer, thus mimicking back-supported flames. Mastorakos *et al.* [11] used an asymmetric configuration for experiments to study the mixing of products and unburned reactants. In their study, the authors concluded that premixed flames would not reach extinction due to high bulk strain rates as long as the temperature of the hot products was greater than 1550 K. Coriton *et al.* [15] varied the composition and temperature of the hot product stream in an asymmetric counterflow flame experiment. For a lean reactant mixture with products from a stoichiometric premixed flame, the temperature of the hot products had a significant impact on the heat release rate at varying strains. As the temperature of the burned products increased, the heat release rate also increased. With increasingly bulk strain values, the heat release rate could be increased by increasing the temperature of the hot products. They also found that the locations and rate of production for various species within the flame would change as the bulk strain rate increased. For example, the fuel consumption layer broadened and the rate of production for CO, CO_2, OH, and H decreased with increasing strain. Additionally, the net rate of reaction for key reactions changed with strain. One reaction they examined that is relevant to the data presented in this study was the change in $CO + OH \rightarrow CO_2 + H$. As the bulk strain increased from 175 s^{-1} to 1100 s^{-1}, the net reaction rate decreased significantly.

In combustion experiments, laser-induced fluorescence (LIF) techniques are often used to collect data on specific species in turbulent flames. Species that are commonly used with LIF include OH, CH, CH_2O, and CO. When assuming a steady laminar flamelet model, the maximum gradient of OH is used as an identifier for the flame edge and the CH molecule is used to locate the reaction zone. LIF data for CH_2O molecules is used as a marker for the preheat zone of the flame and when overlapped with OH LIF data, can be used to distinguish the reaction zone. The

CO molecule LIF data can provide information on where the final recombination reactions occur and on the overall combustion efficiency. Several previous experiments have been completed using LIF data to study turbulent flames [2]–[6], [13]. In addition to collecting LIF data to gain an understanding of the flame structure, simultaneously collected LIF data can be used to determine the rate of reaction of key combustion reactions. In a study on turbulent counterflow premixed flames by Coriton *et al.* [13], LIF data for four different species was collected to produce the forward reaction rates for two key reactions. LIF data for CH_2O and OH was collected simultaneously for the forward reaction rate for $CH_2O + OH \rightarrow HCO + H_2O$. Simultaneous LIF data for CO and OH was used for the forward reaction rate of $CO + OH \rightarrow CO_2 + H$. These reactions provide additional information that can be used when analyzing the structure of the flame. For example, the peak reaction rate of $CH_2O + OH \rightarrow HCO + H_2O$ can be linked with the primary peak heat release for methane-air mixtures that are lean or stoichiometric. The reaction $CO + OH \rightarrow CO_2 + H$ also accounts for a large portion of the heat release and is a dominant reaction in the oxidation layer.

Premixed turbulent combustion data collected in these laser-induced fluorescence experiments is typically interpreted using the steady laminar flamelet model to identify specific regions within the flame structure. The laminar flamelet model assumes that reactions occur in a very thin one-dimensional layer within the flow field. The flame or reaction zone itself is assumed to be small in comparison to the preheat zone that proceeds the flame. In the preheat zone, radicals are formed by chain-branching reactions. These radicals are then consumed in the reaction layer where the flame is present [16]. The steady laminar flamelet model is theoretical concept used for interpreting data in laboratory experiments. In order to use the steady laminar flamelet model to interpret turbulent combustion data, several assumptions are commonly made. The first assumption is that a steady laminar flamelet model can be used to interpret data for an unsteady turbulent flame. While the structure of a premixed flame is affected by the strain imposed on that flame, it is also dependent on the time over which that strain is imposed. For example, very high strain rates imposed for very short timescales do not extinguish flames, as was shown in direct numerical simulation by Im *et al.* [17]. As such, there remain questions about whether a steady simulation is representative of an unsteady flame and whether or not we can use these steady simulations to interpret our diagnostic results. The second assumption is that the reaction zone of the flame is smaller than the turbulence eddies and the third assumption is that the time scale of those eddies is greater than the chemical time scale of the combustion reactions [2]. In addition to those assumptions, it is unknown what effect back-support pilot flames have on both the structure of the flame and the behavior. If back-support pilot flames have a significant impact on the structure or behavior of premixed turbulent flames, a steady laminar flamelet model may not be an appropriate model to use when interpreting data.

The goal of this study is to determine and evaluate a "diagnostic Damköhler number" to help identify if the steady strained flamelet model should be used to interpret data from laser-induced fluorescence measurements. This paper begins by identifying stain rates and durations of those strain rates from previously conducted experiments using a back-supported Bunsen flame [18]. Then, Chemkin simulations of an asymmetric counterflow flame are used to mimic the back-supported flame from the experiments. The asymmetric configuration includes a jet of premixed methane-air reactants and a jet of burned products from a stoichiometric methane-air flame. The velocity of the jets is varied but kept symmetric to create a range of steady strain rates. Data on the location and mole fraction of various species are tracked along with the reaction rates of key reactions. Using the reaction rates from the Chemkin simulations and the residence time of the strains from the experimental data, the diagnostic Damköhler number is developed. In this study, a high Damköhler number would be representative of a quasi-steady strain rate in comparison to the chemical timescale while a small Damköhler number would indicate the opposite. In cases where the Damköhler number is high, it would indicate that the steady flamelet model is an appropriate model to use when interpreting LIF data. However, low Damköhler numbers call into question that interpretation of these diagnostics.

III. Experimental Setup, Diagnostics, and Simulation

A. Experimental Setup

The experimental facility consists of two identical burners with 100 mm x 10 mm exit planes (Figure 1). Each burner consists of two stacked sections (178 mm and 160 mm tall) that contain the inlet for the incoming flow, two layers of ceramic honeycombs and two perforated plates. Mixtures of air and natural gas flow through the two layers of ceramic honeycomb inside the burners that condition the flow before the mixture reaches the two perforated plates. These plates are located 30 mm and 10 mm upstream of the burner exit and each plate has an open area of 40% with hole diameter of 3.18 mm. These perforated plates result in generation of averaged non-reacting flow turbulence-intensities of 18% at the burner exit. More details of the burner are can be found in Ref. [18]. Each burner is also equipped with two types of pilot flames: (i) small "anchoring" pilots, and (ii) "back-support" pilots. The "anchoring" pilots are located close to the exit of the burners and help in anchoring the flames the burner walls, and the larger "back-support" pilots provide adiabatic or super-adiabatic combustion products around the flames to avoid any ambient air entrainment.

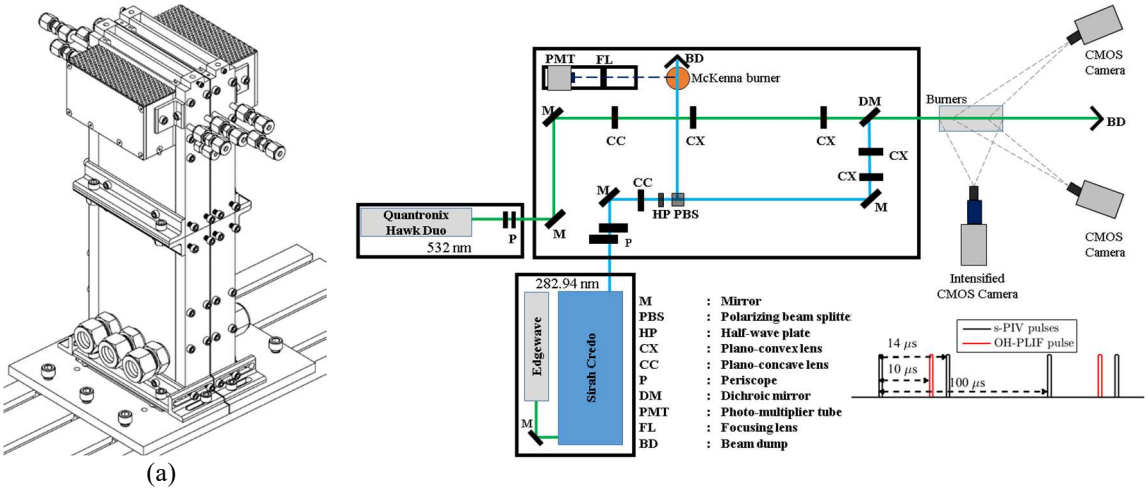

(a) (b)

Figure 1. (a) Isometric view of the dual-burner experiment. (b) Schematic of the simultaneous s-PIV / OH-PLIF laser diagnostic setup

B. Diagnostics

B.1. OH-Planar Laser-Induced Fluorescence (OH-PLIF)

High-speed planar laser-induced fluorescence (PLIF) is used to measure the distribution of the hydroxyl (OH) radicals. A 10 kHz acquisition-rate system is used that consists of a 532 nm Nd:YAG laser (Edgewave) pumping a dye laser (Sirah Credo). The dye laser is tuned to the Q1(6) line of the $A^2\Sigma^+ \leftarrow X^2\Pi$ (1-0) excitation band to excite OH radicals with a wavelength of 282.94 nm. This particular transition for OH radicals is commonly used for flame edge detection and has a discernible peak for varying temperatures and pressures. The maximum pulse energy obtained from the dye laser at 10 kHz repetition-rate is 0.3 mJ/pulse. The UV beam from the dye laser is passed through a periscope and a set of three cylindrical lenses to obtain a collimated sheet with an approximate height of 21 mm. A CMOS sensor camera (Photron FASTCAM SA1.1), coupled with an external intensifier (LaVision HS-IRO) and a 100 mm f/2.8 UV lens (Cerco) is used with a high transmissivity interference filter (LaVision 1108760 VZ) to collect the signal at 320 nm. The field of view achieved through this setup is 50 mm x 100 mm. The intensifier gate is set at 100-150 ns to reduce background flame luminosity.

B.2. Stereoscopic-Particle Image Velocimetry (s-PIV)

A high-speed, dual cavity, Nd:YAG laser (Quantronix Hawk Duo) is utilized to perform stereoscopic-particle image velocimetry at 10 kHz at 532 nm. Similar to the OH-PLIF laser system, a set of collimating optics are used to create a laser sheet with a final height of 50 mm. A pair of CMOS sensor cameras (Photron FASTCAM SA5) equipped with 100 mm f/2.8 lenses (Tokina Macro) and Nikon tele-converters are used to achieve high-resolution images. The angle between the laser sheet plane and each camera sensor is about 25 degrees. The field of view obtained through this setup is 32 mm x 53 mm. The flow-field is seeded with 0.5-2 micron-sized aluminum oxide particles, and 532 nm laser-illuminated images are collected at 10 kHz in double frame mode, with a pulse separation of 14 μs. Near-infrared filters (Schneider Kreuznach IR MTD) and laser line filters (Edmund Optics TECHSPEC 532 nm CWL) are used on each camera to reduce measuring the effects of flame luminosity. Vector calculations are performed using DaVis 8.3 from LaVision using a multi-pass algorithm is used with window sizes ranging from 64 x 64 to 16 x 16. For each pass, a 50% overlap is used and the resulting vector spacing is 0.48 mm/vector. Post-processing of vectors is performed with a universal outlier detection scheme, with a 3x median filter. Using the uncertainty calculation feature in DaVis 8.3, averaged uncertainties in instantaneous velocities range from 1.4 - 2.5 m/s in the jet region of the burners for U=12 - 28 m/s.

C. Simulation

Using the Opposed Flow Flame simulation (OPPDIF) in Chemkin, burners with back-support pilot flames were simulated using an asymmetric counterflow flame configuration. The asymmetric configuration uses two jets with matching exit velocities and varying mixtures. The first jet contains a stoichiometric mixture of methane-air reactants

at 300 K and atmospheric pressure, mimicking the reactant stream from the Bunsen burners. The composition of the second jet is based on the equilibrium products from a stoichiometric methane-air flame in order to mimic the back-support flames. Chemkin's Equilibrium Solver was used to determine the composition and temperature of the methane-air reaction. The sixteen species with the largest mole fractions were used as the composition of the product stream at a temperature of 2225.1 K. The sixteen product species and their mole fractions are shown in Table 1.

Table 1. Product Stream Species

Species	Mole Fraction	Species	Mole Fraction
N_2	0.708698	H	3.89×10^{-4}
H_2O	0.183411	O	2.15×10^{-4}
CO_2	0.085349	HO_2	4.98×10^{-7}
CO	0.008971	NO_2	3.46×10^{-7}
O_2	0.004614	N_2O	1.00×10^{-7}
H_2	0.003598	H_2O_2	4.56×10^{-8}
OH	0.002869	HNO	3.36×10^{-8}
NO	0.001885	N	1.42×10^{-8}

The distance between the nozzle exits was set at 1.4 cm with a maximum number of grid points of 2000 in order to ensure convergence in each case. The use of the OPPDIF simulation simulates a back-supported flame by modeling the thermal and species diffusion across the premixed reactants region and the burned reactants region. The bulk strains values used in this paper are calculated based on the jet velocity at the output of the nozzles in the Chemkin OPPDIF simulation. The bulk strain values are calculated using Eq. (1), where v is the velocity of the jet at the nozzle exit and d is the distance between the nozzles.

$$K_{Bulk} = \frac{2v}{d} \tag{1}$$

The temperature of the first nozzle is set to the temperature of the premixed reactants and the temperature of the second nozzle is set to the equilibrium temperature of the products. The mechanism used in the Chemkin simulations was GRI-Mech 3.0 [19]. The parameters used for the Chemkin simulations discussed in this paper are shown in Table 2, where T_1 is the temperature of the premixed reactants, T_2 is the temperature of the burned reactants at the nozzle exit, and v is the velocity of both jets at the nozzle exit. For the purpose of this paper, the equivalence ratio of the premixed reactants was kept at 1.0 and the composition of the burned products jet was based on the output from the Equilibrium Solver for a mixture with an equivalence ratio of 1.0. This aligns with the equivalence ratio of the main and pilot flames in the experiment.

Table 2. Chemkin simulation cases

Run #	T_1 (K)	T_2 (K)	v (m/s)	Bulk strain (1/s)	Equivalence Ratio
1	300	2225.132	3	428	1.0
2	300	2225.132	4	571	1.0
3	300	2225.132	5	714	1.0
4	300	2225.132	6	857	1.0
5	300	2225.132	7	1000	1.0
6	300	2225.132	8	1142	1.0
7	300	2225.132	9	1285	1.0
8	300	2225.132	10	1428	1.0
9	300	2225.132	11	1571	1.0
10	300	2225.132	12	1714	1.0
11	300	2225.132	13	1857	1.0
12	300	2225.132	14	2000	1.0
13	300	2225.132	15	2142	1.0
14	300	2225.132	20	2857	1.0
15	300	2225.132	25	3571	1.0
16	300	2225.132	30	4285	1.0
17	300	2225.132	100	14285	1.0

The velocities in the simulation from 3-30 m/s were chosen to capture the bulk strain ranges found in the experiments, as shown in Figure 2b. The 100 m/s case is far beyond any strains measured in the experiment but was run to demonstrate the interesting "non-extinguishing" behavior of back-supported strained flames. In these cases, as will be discussed, the heat release rate does not go to zero despite the bulk strain rate being far beyond that of the extinction strain rate of a non-back-supported flame. Implications for this trend are discussed in the results as it relates to LIF diagnostics.

IV. Results

A. Fluid strain rates

From the s-PIV measurements, strain rates can be extracted ahead of the flame front region. For the purpose of the current study, a time-averaged progress variable location of 0.1 is chosen to calculate strain rates in the Cartesian frame of reference using the following equations:

$$S_{ij} = \begin{cases} S_{12} = \frac{1}{2}\left(\frac{\partial U_x}{\partial y} + \frac{\partial U_y}{\partial x}\right) \\ S_{11} = \frac{\partial U_x}{\partial x} \\ S_{22} = \frac{\partial U_y}{\partial y} \end{cases} \quad \textbf{(2)}$$

Figure 2a shows the location of the progress variable in a dual-flame configuration, which has been discussed in our previous work [18]. Figure 2b shows the probability density function (PDF) of instantaneous strain rates along the $\bar{c}$=0.1 contour, indicating that the highest strain rates measured were on the order of 5000 1/s; this range of strain rates is used in the OPPDIF simulation. These very high levels are strain are evidence of the significant role that back-support pilot flames play in stabilizing the flame and maintaining the flamelet structure in operational regimes where traditional theory like the Borghi-Peters diagram would predict broken flamelets.

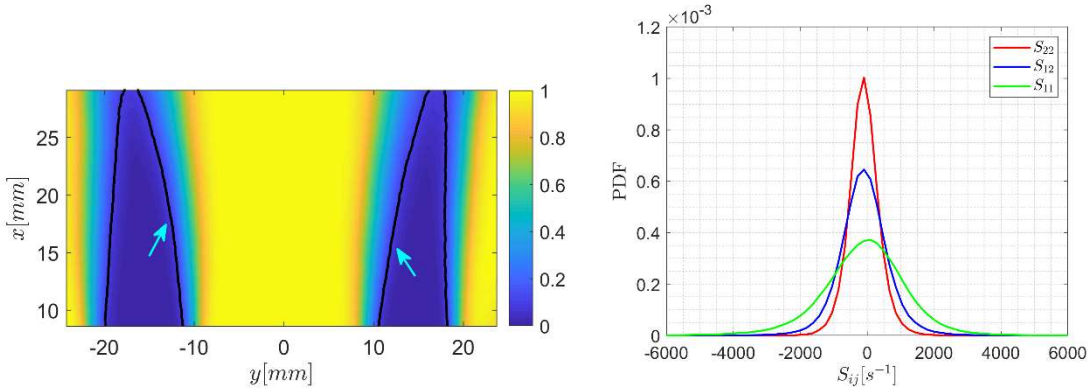

Figure 2. (a) Time-averaged progress variable of dual-burner flames operating at U = 12m/s. The black-contours represent the $\bar{c}$=0.1. (b) PDFs of strain rates along the $\bar{c}$=0.1 of the left flame

B. Impact of strain on chemical species measured by LIF and heat release

Using Chemkin's OPPDIF model, key features for each of the cases presented in Table 2 can be extracted. The peak heat release rate for each bulk strain case is shown Figure 3. The red line and the red dot show the extinction strain rate and heat release rate, respectively, for the symmetric OPPDIF scenario where both nozzles emit reactants at 300 K. Extinction using the symmetric configuration was clearly indicated by very little temperature increase and nearly zero net heat release. For the asymmetric OPPDIF cases, as the bulk strain increases the peak heat release rate decreases. However, even at very high strain rates, the peak heat release rate does not reach zero as would be expected with flame extinction. The peak heat release rate appears to asymptote to approximately 250 J/cm^3/s at high strains, which is over an order of magnitude less heat release than in the unstrained case. This sustained heat release suggests that even at very high strains, reactions are continuing to occur and would be visible using a LIF diagnostic like OH- or CH-PLIF. To understand how those LIF signals might change with strain, the mole fraction for several LIF species

was extracted and plotted. The peak mole fractions of CH_2O, CO, OH, and CH, all important LIF species, are shown in Figure 4. CH_2O, OH, and CH are plotted on the left axis; CO is plotted on the right axis.

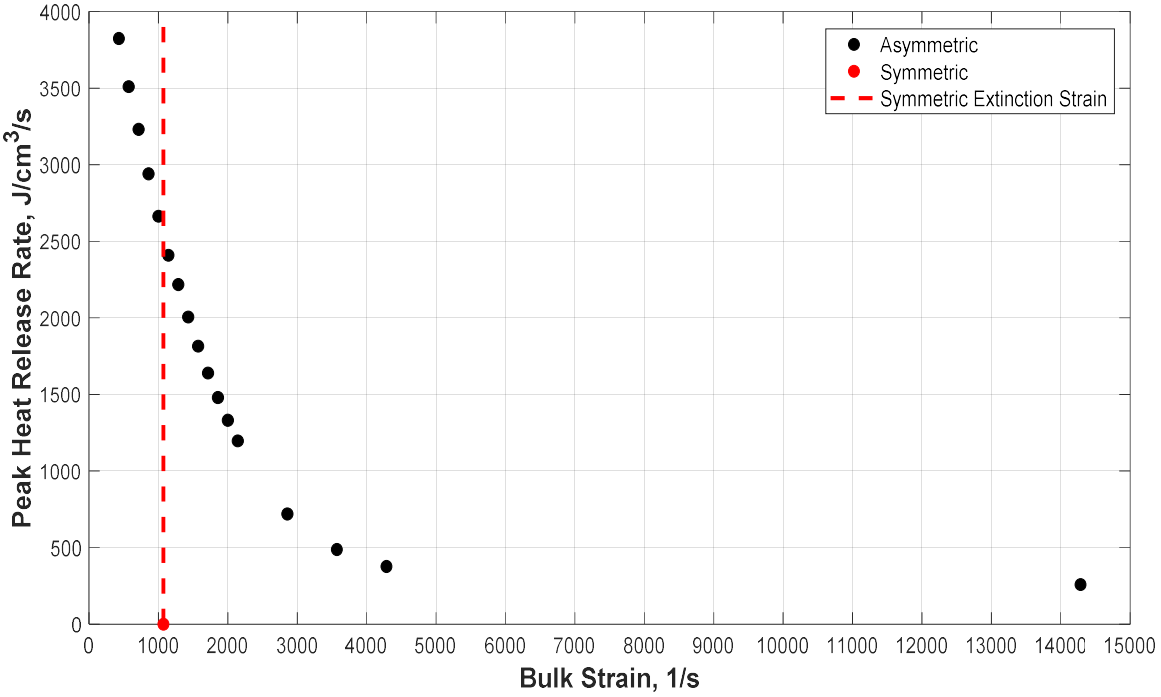

Figure 3. Peak heat release rate as a function of bulk strain

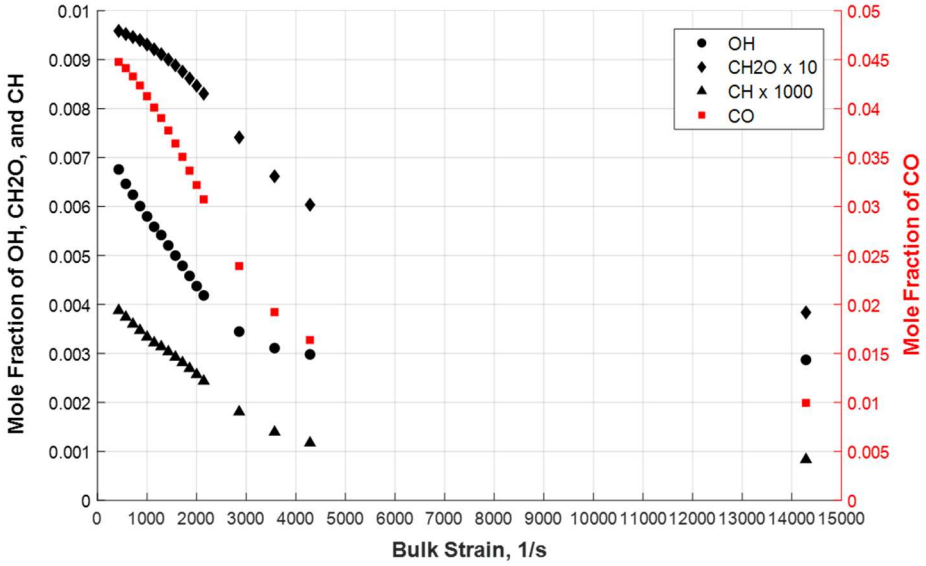

Figure 4. Peak mole fractions of LIF species versus bulk strains

For all four species, the peak mole fractions gradually decrease as the bulk strain increases. Notably, the mole fractions of OH and CH both demonstrate the same asymptotic behavior as the net heat release rate while the mole fractions of CH_2O and CO continue to gradually decrease at all strain levels. As the bulk strain increases, the amount of OH being produced decreases until the maximum mole fraction of OH becomes the same as the OH present in the hot products. At the largest bulk strain, the peak mole fraction of OH is about 0.0029 and the mole fraction of OH in the burned products was 0.002869. Similar to OH, the peak mole fraction of CO at the highest strain also decreased

to around the same fraction present in the burned products. For the CO specie, the peak mole fraction at the highest strain rate was about 0.01 and the mole fraction of OH in the burned products was 0.008971.

Interestingly, the species CH_2O and CH were not included in the top 16 most plentiful species of the burned product stream, but these species were both present at the high strain rates. The species CH_2O and CH are associated with the preheat and reaction zones in a steady laminar flame. Their presence at the high strain rates suggests that there could be a flame structure present with reactions continuing even with the very high strain. The presence of additional CH_2O and CO is likely due to incomplete combustion occurring at the extremely high strain rates. Typically, OH would also be considered an indicator of incomplete recombination reactions after the high heat release reactions. Since the peak mole fraction of OH approaches the mole fraction of OH in the burned products at very high strain values, it is difficult to tell what the source of the OH is at those levels. The presence of CO specifically is indicative of the fact that reaction has not ceased despite the high levels of strain. For all the species the peak mole fraction occurs at the smallest bulk strain ($K_{bulk} = 428$).

Comparing the rates at which the peak mole fractions decrease with increasing bulk strain, the peak mole fractions of CH_2O and CH decrease at a more gradual rate as the bulk strain increases than the peak mole fractions of OH and CO. In measuring a flame, CH LIF data is typically used to indicate where the reaction zone and peak heat release is occurring. In the simulation, the presence of CH combined with the data indicating heat is being released at the high strain rates further supports the idea that reactions are present at the high strain rates. One possible reason as to why radicals associated with flamelet structures are found at even the very high levels of strain could be due to the adiabatic shield created by the back-support pilot flames. The pilot flames not only create a layer of hot products to prevent heat loss, but they also create a pool of radicals that interact with the premixed reactants. The pool of radicals formed by the back-support pilot flames could be supporting combustion reactions at the high strain levels that would otherwise be able to occur. It may be that the pool of radicals from the hot products are enough to support a reaction in a turbulent environment where a flame could not create an explosive mixture due to the high levels of strain and heat loss without a back-support pilot. Another potential issue to consider is the presence of the LIF species in the hot products from the back-support pilot flames. As these species are used to identify regions where key reactions occur, there is a risk that LIF data could be misinterpreted due to the species already existing in the hot product stream.

In addition to changing the peak mole fraction, the increasing strain also changes the location where the peak mole fractions and peak heat release occur. Figure 4 shows the peak mole fraction of the four LIF species and the heat release rate as a function of their location; the colorbar shows the bulk strain at each location and the dotted line indicates where the stagnation plane is located. In these figures, the stagnation plane occurs at about 1.028 cm with the exit plane of the reactant jet located at 0 cm and the exit plane of the burned products jet located at 1.4 cm. As the strain increases, the location of the peak values shifts away from the reactant nozzle and towards the stagnation plane. The locations of the peak mole fractions of OH, CH, and CO eventually cross the stagnation plane and into the hot products region. The location of the maximum heat release rate also shifts from the premixed reactants region and into the hot products region.

At even higher strain rates, the location of the net heat release rate, peak CH mole fraction, and peak CO mole fraction shifts back towards the reactants side. In contrast, the location of the peak mole fraction of CH_2O never crosses the stagnation plane and the location of the peak mole fraction of OH never shifts back towards the reactants side after crossing the stagnation plane. The shift in the location of the peak heat release and CH across the stagnation plane while CH_2O never crosses into the burned products region describes how the flame structure is shifting as the strain increases. The CH_2O is an indicator that the preheat zone remains in the reactant region even at very high strain, while the reaction zone moves into the burned products region. Building on the idea mentioned above, this could be further indication that the pool of radicals in the burned products may be enough to support combustion reactions even at very high strains where a preheat zone is unable to exist. The first interaction between the radicals from the back-support pilot flame would be at the stagnation plane and at a small distance away as diffusion occurs. The existence of species associated with the preheat zone and not present in the burned products is indicative that there is a form of a preheat zone occurring around the stagnation plane.

C. Impact of strain on chemical reaction rates

The high strain rates affect not only the peak mole fractions, but also the rate and direction of the dominant reactions related to the production of these key LIF species. Three reactions were considered due to their relationship with species used with LIF measurements and their use in previous LIF studies [2]–[6], [13]: $HCO + O_2 \leftrightarrow CO + HO_2$, $CH_2O + OH \leftrightarrow HCO + H_2O$, and $CO + OH \leftrightarrow CO_2 + H$. These reactions are dominant reactions that produce the species OH and CH as well as strongly influencing the net heat release. For each of the three reactions, the net reaction rates were calculated using Chemkin's reaction pathways analysis. The location where the reaction rate data was collected was based on the location of the peak mole fractions of OH, CH, and peak heat release rate for each

strain rate case. The maximum gradient of OH was also selected as a location to collect reaction rate data. These locations were chosen for their relevance to LIF imaging; the peak CH mole fraction and maximum gradient of OH are common methods of identifying flame edges in CH- and OH-PLIF imaging, respectively. The other two locations are interesting for chemical, rather than diagnostic, reasons.

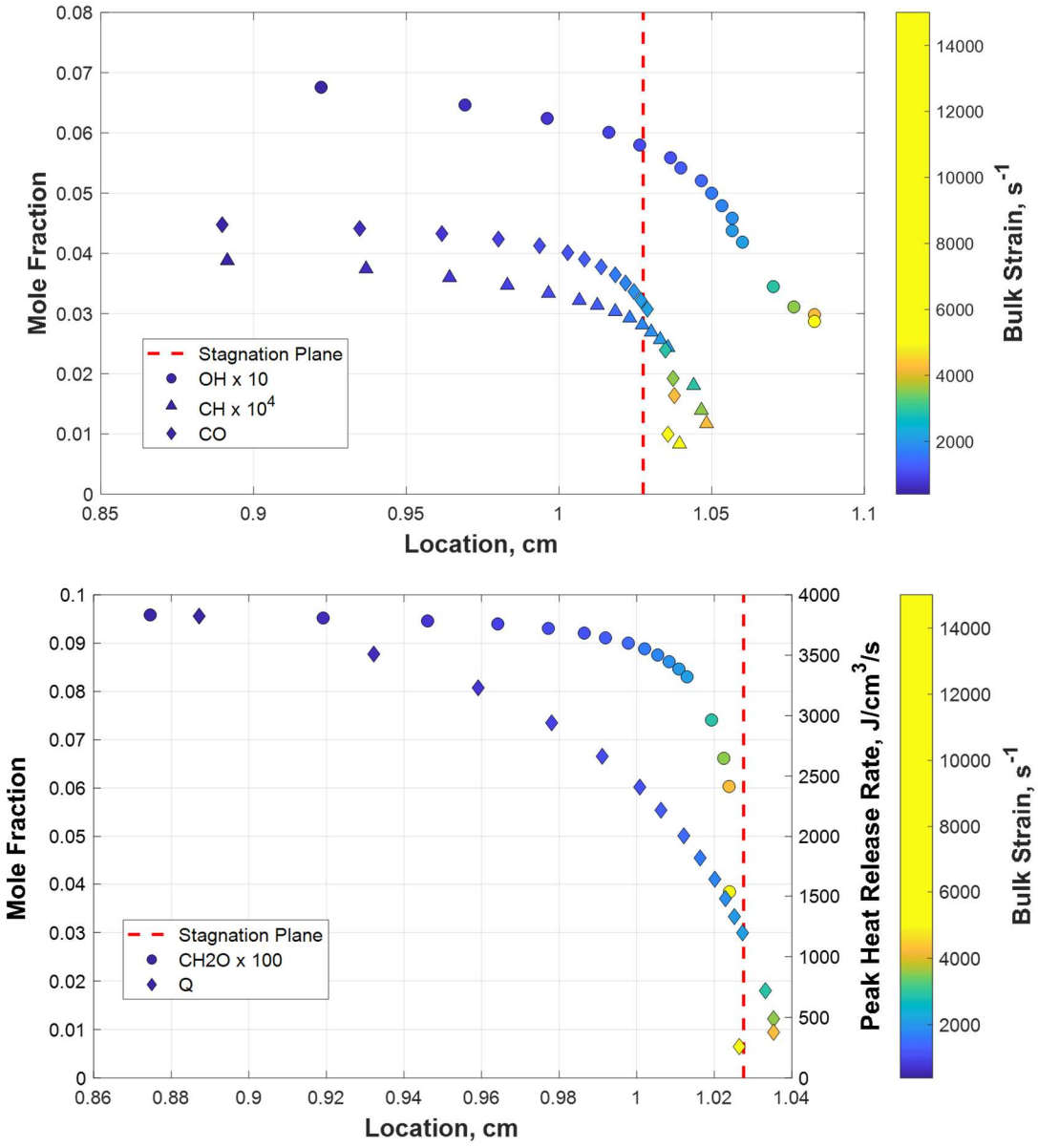

Figure 4. Location of peak mole fraction and heat release rate for each bulk strain rate.

The net reaction rates for $HCO + O_2 \leftrightarrow CO + HO_2$ in terms of the location and bulk strain are shown in Figure 5. In these plots, the color bar indicates the axial location where the measurement was taken. This is significant as it shows if the reaction rate location has crossed the stagnation plane. The stagnation plane location occurred around 1.028 cm. Even at very high strain rates, there is still a net forward reaction rate occurring for the $HCO + O_2 \leftrightarrow CO + HO_2$ reaction. The reaction rate peaks at the lower strain rates and then begins a gradual decrease as the strain increases. The $HCO + O_2 \leftrightarrow CO + HO_2$ reaction is a key reaction in the production of CO and has been used in LIF imaging as an indicator of final recombination reactions [13]. The forward reaction rate of this reaction even at high strains is significant as it indicates incomplete combustion. Additionally, the largest reaction rate at the highest strain level occurred at the peak heat release location. As discussed in the previous section, the peak heat release rate shifted

out of the reactant region and into the burned products at the high strain rates. The existence of this reaction combined with the presence of CH in the burned product zone further suggests the reaction zone is occurring in the burned products region at very high strain rates.

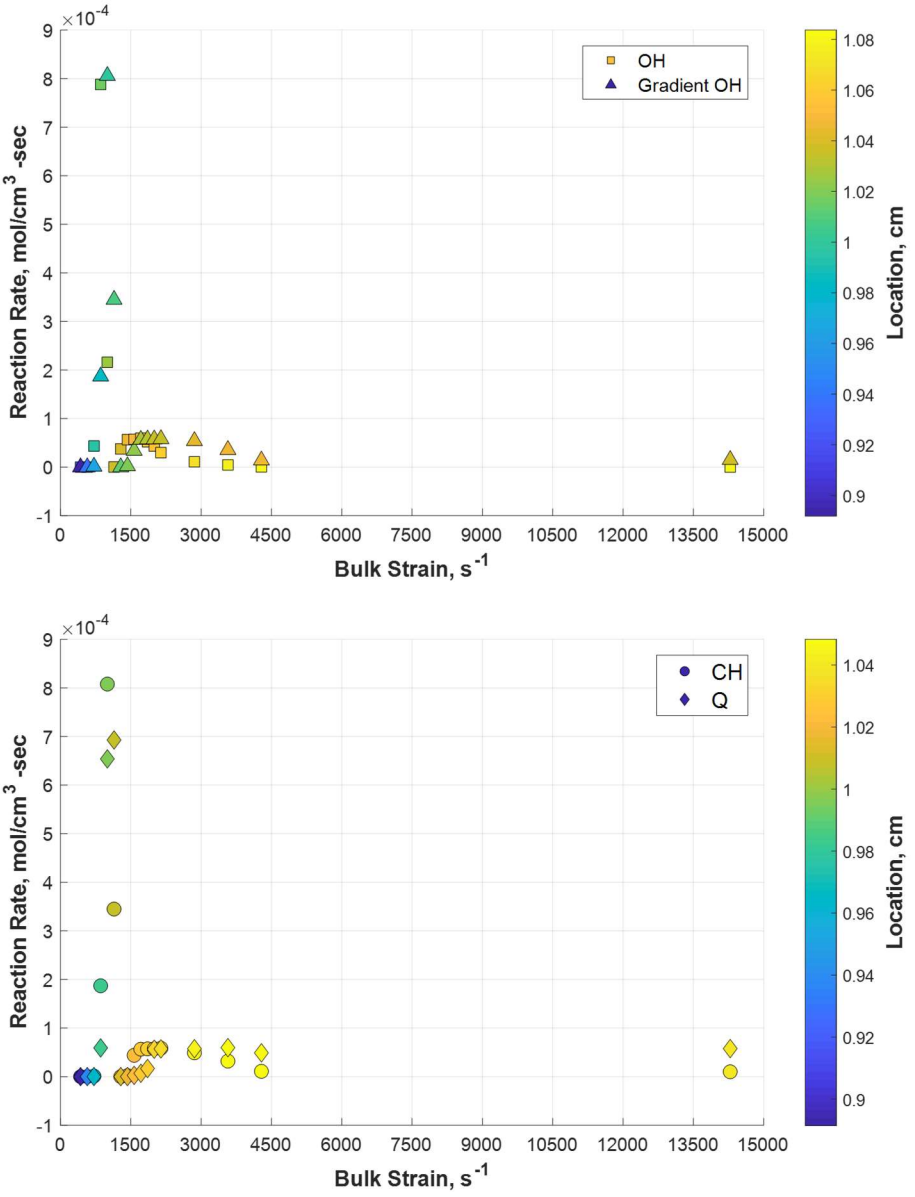

Figure 5. Location of peak reaction rate of $HCO + O_2 \leftrightarrow CO + HO_2$ at varying bulk strain rates at peak OH, peak gradient OH, peak CH, and peak heat release rate (Q) locations.

The net reaction rates for $CH_2O + OH \leftrightarrow HCO + H_2O$ in terms of the location and bulk strain are shown in Figure 6. Similar to the $HCO + O_2 \leftrightarrow CO + HO_2$ reaction, the peak net reaction rate for $CH_2O + OH \leftrightarrow HCO + H_2O$ occurs at lower strain rates. However, the net reaction rate at the peak CH, maximum OH gradient, and net heat release locations experiences another smaller peak between 1500 s^{-1} and 4500 s^{-1}. This second peak happens at the around the strain values at which the peak mole fractions for several species cross the stagnation plane. After the second peak the reaction rate remains relatively constant even at the very high strain rates. The reaction $CH_2O + OH \leftrightarrow HCO + H_2O$ is associated with heat release in a reaction. Interestingly, the second peak reaction rate occurs at about 4500 s^{-1}, which is the strain at which the peak heat release, peak mole fraction of CH, and peak mole fraction of CO begins to shift back towards the stagnation plan and the product stream. The secondary increase in the consumption of CH_2O at the

higher strain indicates incomplete combustion and the existence of a second peak in the reaction zone suggests the combustion reactions continue in the burned products stream as the strain rates become large.

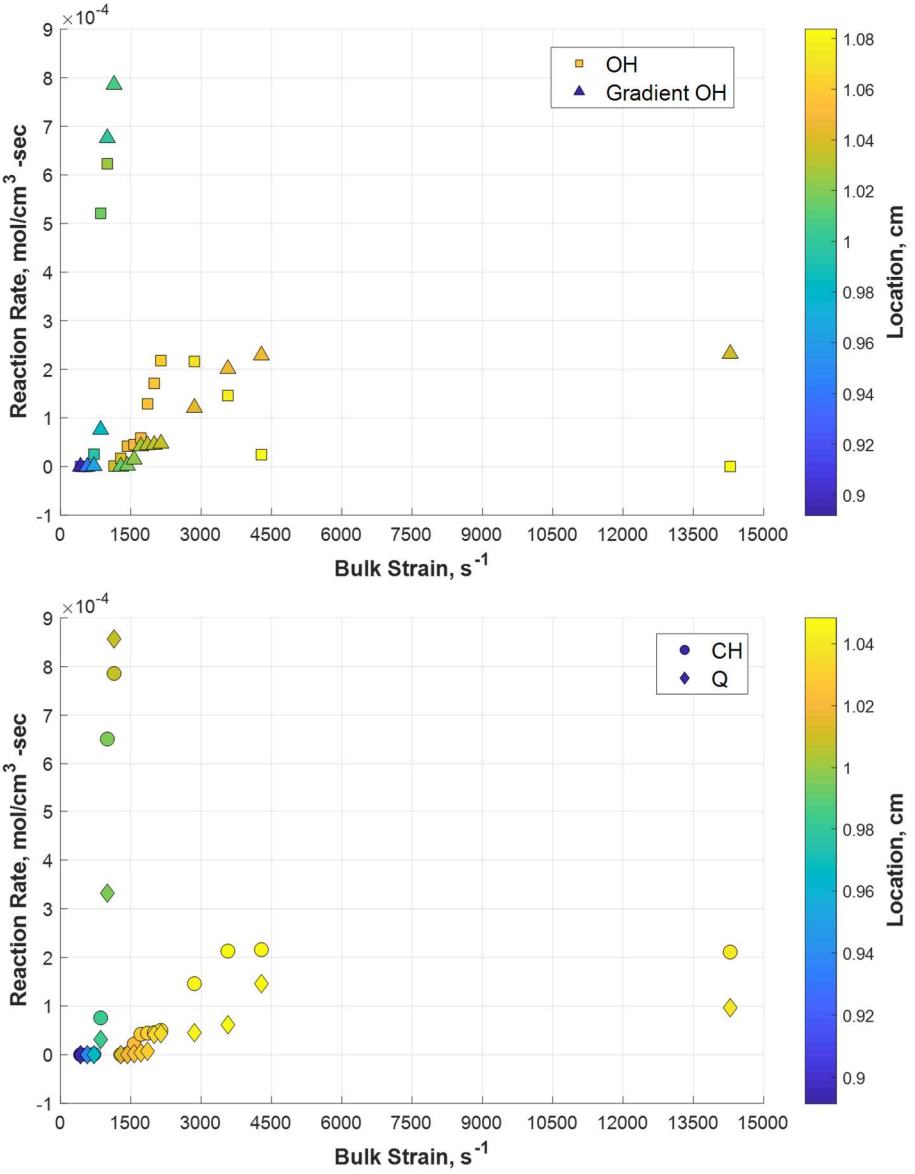

Figure 6. Location of peak reaction rate of $CH_2O + OH \leftrightarrow HCO + H_2O$ at varying bulk strain rates at peak OH, peak gradient OH, peak CH, and peak heat release rate (Q) locations.

The net reaction rates for $CO + OH \leftrightarrow CO_2 + H$ in terms of the location and bulk strain are shown in Figure 7. Similar to the other two reactions already discussed, the peak net reaction rate for $CO + OH \leftrightarrow CO_2 + H$ occurs at lower strain rates, but the gradual decrease as the strain goes up is much smaller than the $HCO + O_2 \leftrightarrow CO + HO_2$ reaction. Almost immediately after the initial peak at the lower strain rates, the reaction rate drops to around zero. However, the reaction rate does not remain zero as the strain rate continues to decrease. At strain rates around 1500 s^{-1} to 14285 s^{-1}, the reaction rate becomes negative. This negative value shows the reaction direction begins to reverse at the higher strain rates. This reversal would create more of the CO and OH radicals instead of consuming them at this location. The $CO + OH \leftrightarrow CO_2 + H$ reaction is associated with heat release in reactions. The relatively small reaction rate combined with the positive net heat release would indicate that this reaction may not remain a key reaction at high strain rates. The reaction pathways at high strain rates could change allowing there to still be heat release when one of the key heat release reactions becomes very small. This reversal also has significant implications for interpretation of LIF results. Previous studies using simultaneous OH- and CO-PLIF to measure the rate of this

reaction in turbulent flames have assumed that the reaction only moves forward [13]. However, these steady results indicate that at high enough strain rates, the reaction may in fact progress the other direction, which would significant change the interpretation of these simultaneous LIF measurements.

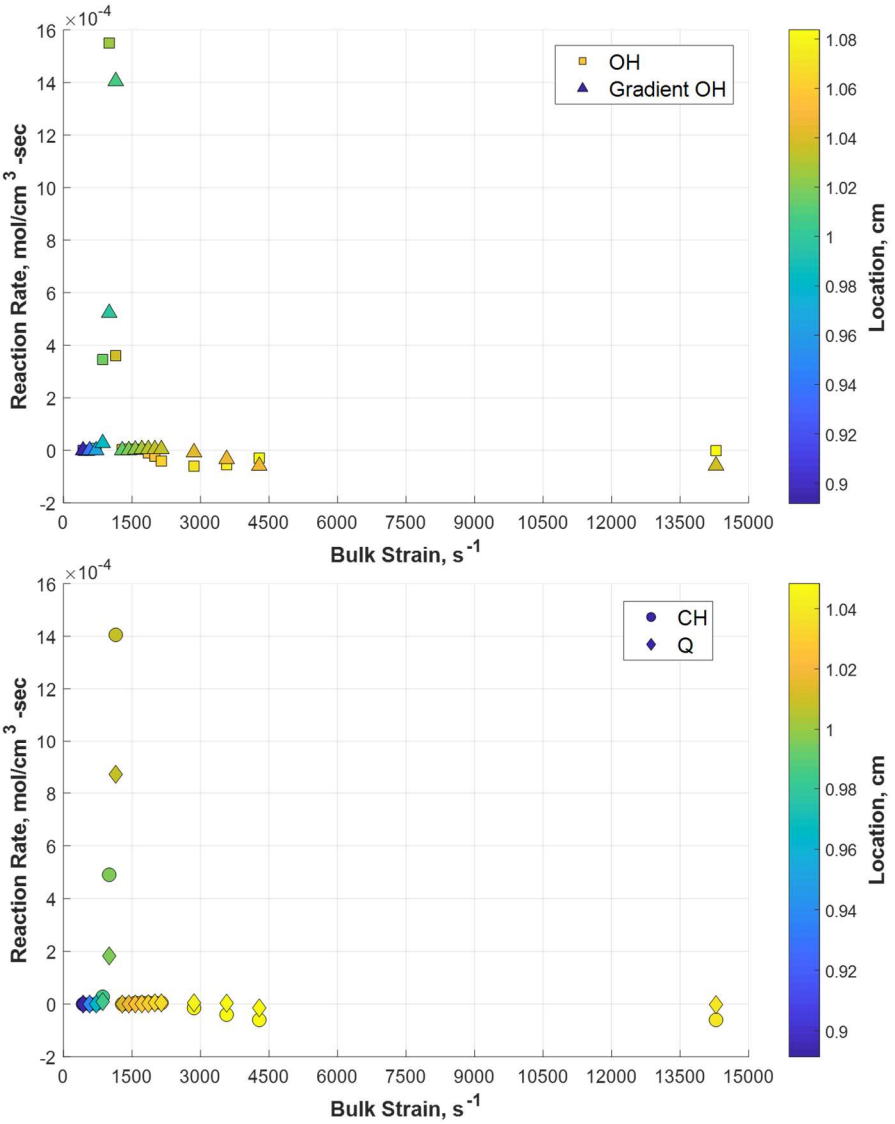

Figure 7. Location of peak reaction rate of $CO + OH \leftrightarrow CO_2 + H$ at varying bulk strain rates at peak OH, peak gradient OH, peak CH, and peak heat release rate (Q) locations.

An interesting relationship between the net reaction rates and the peak species mole fractions is that they all demonstrate a similar asymptotic behavior as the strain reaches very high levels. For the species mole fractions, some of the asymptotic behavior was driven by the composition of the burned products. However, not all of the species are contained in the burned products at any meaningful level, indicating that there are reactions occurring to produce those species. The reactions $HCO + O_2 \leftrightarrow CO + HO_2$ and $CO + OH \leftrightarrow CO_2 + H$ asymptote to a very small reaction rate, but the $CH_2O + OH \leftrightarrow HCO + H_2O$ does not. Even at extremely high levels of strain, the net reaction rate for $CH_2O + OH \leftrightarrow HCO + H_2O$ is still about 20% of the peak net reaction rate at the lower strain values. This continued reaction could be supported by the hot products as OH was one of the eight largest species in the hot product stream. If the OH in the product stream is allowing the $CH_2O + OH \leftrightarrow HCO + H_2O$ reaction to continue, the hot products from the back-support pilot flames would be altering the behavior of the flame at the high strain levels. Additionally, the $CO + OH \leftrightarrow CO_2 + H$ net reaction rate becomes negative at high stain levels meaning the radical OH would be produced instead of being consumed. OH-PLIF is used to identify the flame edge using the maximum gradient of the OH mole fraction. If OH was being produced by $CO + OH \leftrightarrow CO_2 + H$ and being introduced into the mixture from the burned

products, the PLIF data could identify this region as having the maximum gradient of OH. The asymptotic behavior of the reaction rates coupled with the continued presence of key species at high strain rates would suggest that after a certain strain rate is reached, increasing that strain rate has less of an impact on the pathways and peak mole fractions as a result of the back-support.

D. Diagnostic Damköhler number

Results of the OPPDIF simulation showed that the high levels of strain experienced by the flame can have significant effects on the chemical pathways, particularly in the presence of back-support, where we modeled the back-support pilot flames using the asymmetric OPPDIF configuration. In addition to understanding the role of back support on flame structure, one of the motivating questions of this work is whether the steady counterflow paradigm can be used to understand the chemical pathways present in a turbulent flame and whether these pathways can be used to interpret multi-species LIF data. In order to answer these questions, we propose a "diagnostic Damköhler number," which is the ratio of the residence time the fluid spends at a given strain rate versus the chemical timescale from the steady simulation, as in Equation 3.

$$Da_D = \frac{\tau_{res,strain}}{\tau_{chem}} \tag{3}$$

Typically, a Damköhler number would be the ratio of the timescale of the strain itself versus a chemical time, which would indicate whether flame chemical processes could compete with fluid strain processes and sustain combustion. However, this traditional Damköhler number better describes a steady configuration, like the counter-flow flames in the PREMIX simulation, rather than turbulent flames. To understand whether this steady framework can be used to understand processes under these high levels of strain, it is critical to consider not just the magnitude of the strain but the timescale over which the strain operates on the flame. If the time the flame spends at that strain rate is shorter than the chemical timescales associated with a given reaction, then that reaction is not likely to be affected by that strain (Da_D<1). However, if Da_D>1, then the strain is applied over a sufficient time for the chemistry to be altered. Further, use of the steady flame structure and information about the chemical pathways from the steady simulation should only be applied in cases where Da_D>1. In the next section, we plot the chemical timescales (y-axis) vs. the strain residence times (x-axis) with a Da_D=1 line to indicate the border between these two zones. Points that lie above and to the left of the line indicate that Da_D<1 and the steady laminar flamelet simulation is not representative of the physical system. Points that lie below and to the right of the line indicate that Da_D>1, where the simulation is reasonable as the chemical timescales are much shorter than the strain residence timescales and so the chemical reactions can complete at a given level of strain.

To quantify the strain residence times, the strain-rate norm was calculated along the $\bar{\boldsymbol{c}}$=0.1 contour, as shown in Figure 2a, using the method proposed by Wabel *et al.* [20]. This contour was chosen as it is representative of the incoming turbulence ahead of the flame and the PIV measurements are not likely to be biased by the expansion across the flame. Along the contour, we calculated the strain-rate norm in 9x9 pixel, non-overlapping regions at each instant in time for both the left and right flame in the dual-burner configuration. From these data, we defined bins of strain rate (width of ±25 s^{-1}) around the same steady strain levels tested in the Chemkin analysis. Histograms of the residence time of each of these strain bins at the $\bar{\boldsymbol{c}}$=0.1 are shown in Figure 8 for the left flame; the right flame results are very similar and are not shown.

These results show that that the most frequent residence time for any strain rate is only one inter-frame time of the 10 kHz data acquisition. Following similar analysis by Coriton and Frank [21], we ignore the single-frame residence times and average the residence time within each bin. Figure 9 shows these averaged residence time versus the strain rate norm of each bin for both the left and right burner; results from both burners match. These results show that as the strain rate norm increases, the residence time of that strain rate decreases, indicating that very high levels of strain do not act on the flame for a long time. It is these strain residence times that are used next to calculate the diagnostic Damköhler number.

Chemkin's reaction pathways analyzer was used to gather the chemical times for three reactions at various locations. Four locations were selected to gather the net reaction rates based on how LIF data is interpreted. The reaction rates were gathered at the location where the peak OH, peak CH, peak net heat release, and maximum gradient of OH occurred. The rates of production reported by Chemkin are in units of mole/cm^3-s. In order to create a dimensionless Damköhler number, the units of the production rates need to be converted to s^{-1}. To achieve this, the rates of production were divided by the mole fraction of the least-populous, or rate-limiting, specie at that measurement location. For example, for a positive rate of production for $CO + OH \leftrightarrow CO_2 + H$ the mole fraction of the smallest specie of CO or OH would be used. The mole fraction was used in this case as it is a measurement of the concentration of a particular species within the mixture. To obtain the chemical time the inverse of the net reaction or the sum of the

forward and reverse reaction rate was taken. As some of the reaction rates were negative, the absolute value was taken of the chemical timescale before the diagnostic Damköhler number calculations were performed.

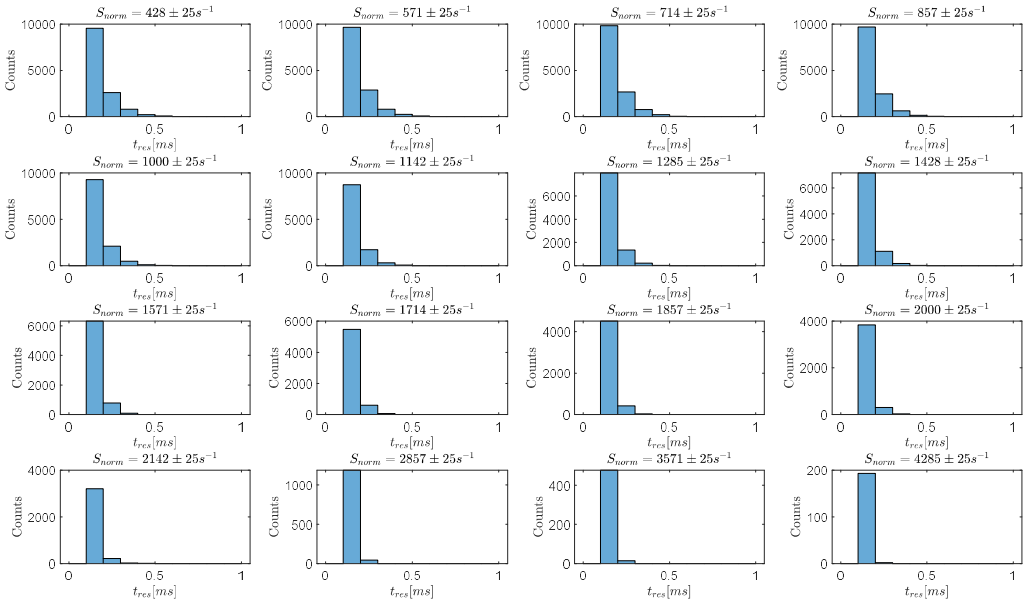

Figure 8. Histograms of residence times for all strain bins for the left flame.

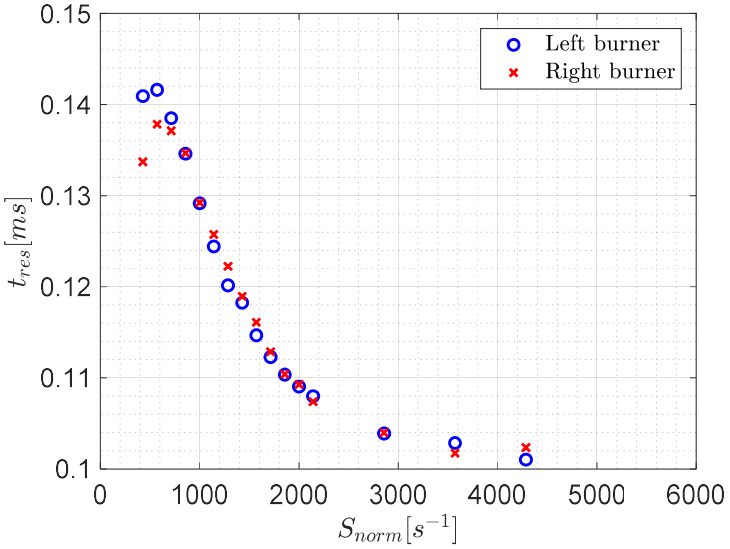

Figure 9. Strain rate residence times at a range of strain rate norms for left and right burner.

Using the residence time of the strain and the reaction rates, the diagnostic Damköhler number was plotted in Figure 10 where the line on each plot represents where the Da_D=1. At each of the measurement locations, the largest chemical timescale occurred at a lower jet velocity of 5 m/s with a bulk strain of about 714 s^{-1}. At the peak CH, net heat release, and maximum gradient of OH locations, a secondary peak occurred at a jet velocity of 9 m/s with a bulk strain of about 1286 s^{-1}. For all four locations, the majority of chemical timescales were significantly slower than the residence time of the strain, which means the reactions are not likely affected by the strain. The one location where the chemical timescale was less than the residence time was at the peak OH location for a jet velocity of 6 m/s and a bulk strain of about 857 s^{-1}. The chemical timescale and average residence time are almost equal at the peak OH location when the jet velocity is 7 m/s with a bulk strain of 1000 s^{-1}.

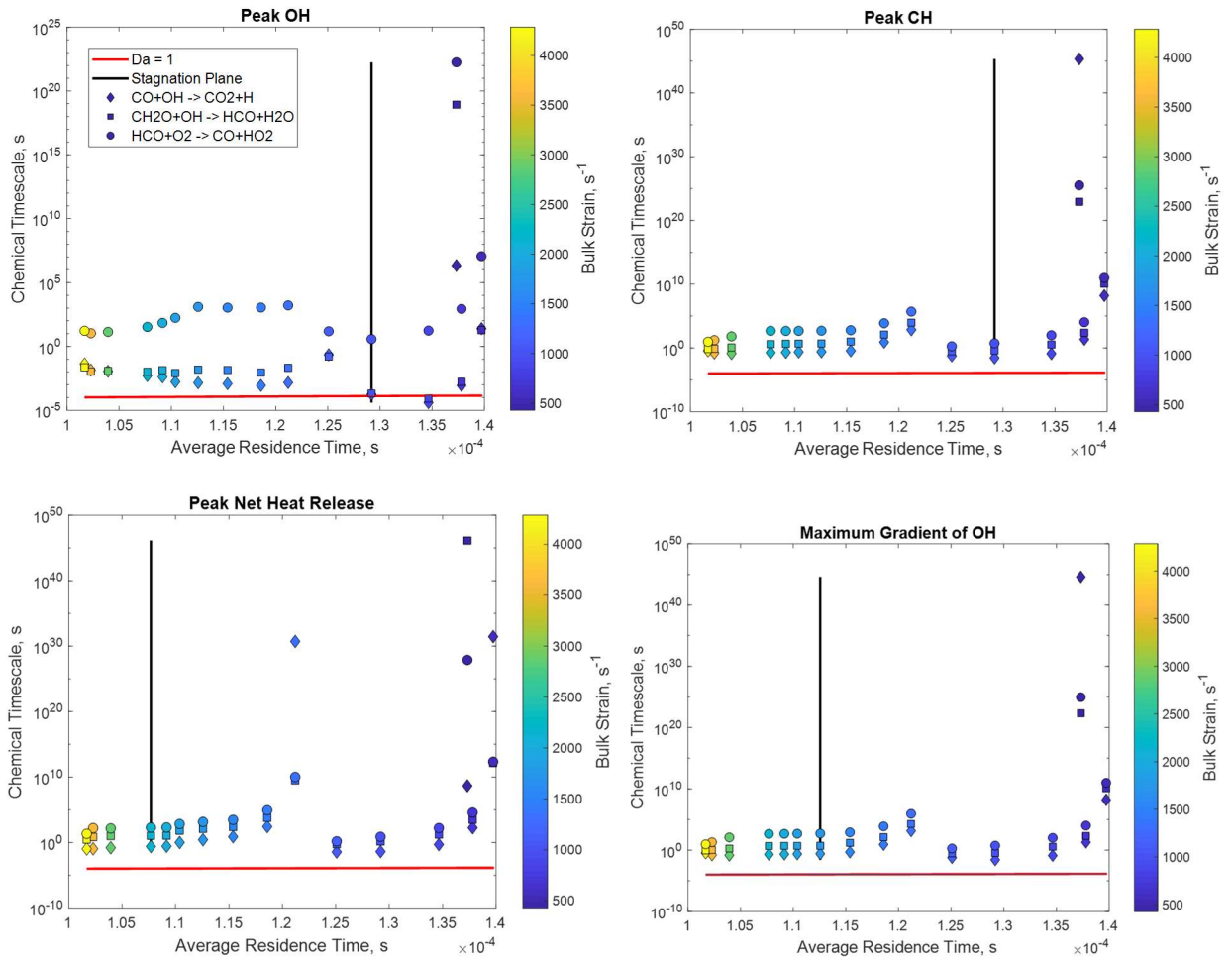

Figure 10. Reaction Rates at Key Locations

To better understand the effect of back-support, a baseline symmetric OPPDIF simulation was run in Chemkin, where each nozzle had a jet of stoichiometric premixed methane-air. In a stoichiometric symmetric OPPDIF simulation for premixed methane-air reactants, extinction occurred between 7 m/s and 7.5 m/s or a bulk strain of about 1000 s^{-1} to 1071s^{-1}. This seems to suggest that using back-supported pilot flames creates a scenario where instead of flame extinction occurring due to strain, chemical reactions are still occurring at a timescale where they are unaffected by the strain. Another interesting feature is the wave-like variations in chemical timescales with strain that occur for the peak CH, net heat release, and maximum gradient of OH measurement locations. At all three of those locations, the largest chemical timescale occurs at a jet velocity of 5 m/s, decreases along a curve, and then increases again to a second peak at a jet velocity of 9 m/s. After 9 m/s the chemical timescale again decreases along a curve and appears to be reaching an asymptote. The largest timescale occurs at the lower jet velocities because the reaction rates at the lower velocities is very small. The mole fraction of the least populous species varies minimally across the bulk strain range in comparison to the reaction rate. Referring back to Figure 5 through Figure 7, it can be seen that the reaction rates do not begin to increase significantly until about 6-7 m/s. Interestingly, that indicates that the reaction rate experiences an increases at around the extinction velocity and bulk strain instead of decreasing as would be expected near extinction.

The one measurement location that did not follow this pattern was the peak OH location. At this location, the reactions $CH_2O + OH \leftrightarrow HCO + H_2O$ and $CO + OH \leftrightarrow CO_2 + H$ also varied, but the secondary peak occurred at 8 m/s. However, the reaction $HCO + O_2 \leftrightarrow CO + HO_2$ experienced the secondary chemical timescale peak at 9 m/s and did not begin to decrease until about 12 m/s. One other difference between the peak OH measurement location data was that the chemical timescale for all three reactions began to increase again after 25 m/s. The reaction rates at the peak OH location shown in Figure 5 through Figure 7 appear to decrease at around that bulk strain rate which would explain the increase in the chemical timescale. It would be expected that the reaction rates would decrease and the

chemical timescale increase as extinction is approached, given the decreasing heat release rate with increasing strain. However, as is shown in Figure 10, that is not the case. The chemical timescales begin to decrease once past the bulk strain at which extinction is expected. The reaction rates for $CO + OH \leftrightarrow CO_2 + H$ reverse at around those strain rates while the reaction rates for $HCO + O_2 \leftrightarrow CO + HO_2$ continue to decrease. The reaction rates for $CH_2O + OH \leftrightarrow HCO + H_2O$ experience an increase at those strain rates except when measured at the peak OH location. Overall, the results show that $Da_D<1$ for the majority of cases, *indicating that the use of the steady laminar flamelet simulation may not be representative of the experiment for the majority of cases*. It should be noted though that between 5-8 m/s and above 11 m/s, the chemical timescales at the peak net heat release rate, maximum gradient of OH, and peak CH begin to approach the strain residence time.

To further explore how the residence time of the strain can alter the flamelet structure, a different approach was used. The three reactions were plotted again with the strain residence time, but instead of looking at the strain values, the location of where the reaction rates were collected is indicated in the colorbar. The plots with this parameter are shown in Figure 11, where the solid black line indicates the last location before the measurement location crosses the stagnation plan. The points to the left of the line are in the burned products region and the points to the right of the line are in the premixed reactants region. The solid red line is where the diagnostic Damköhler number is equal to one.

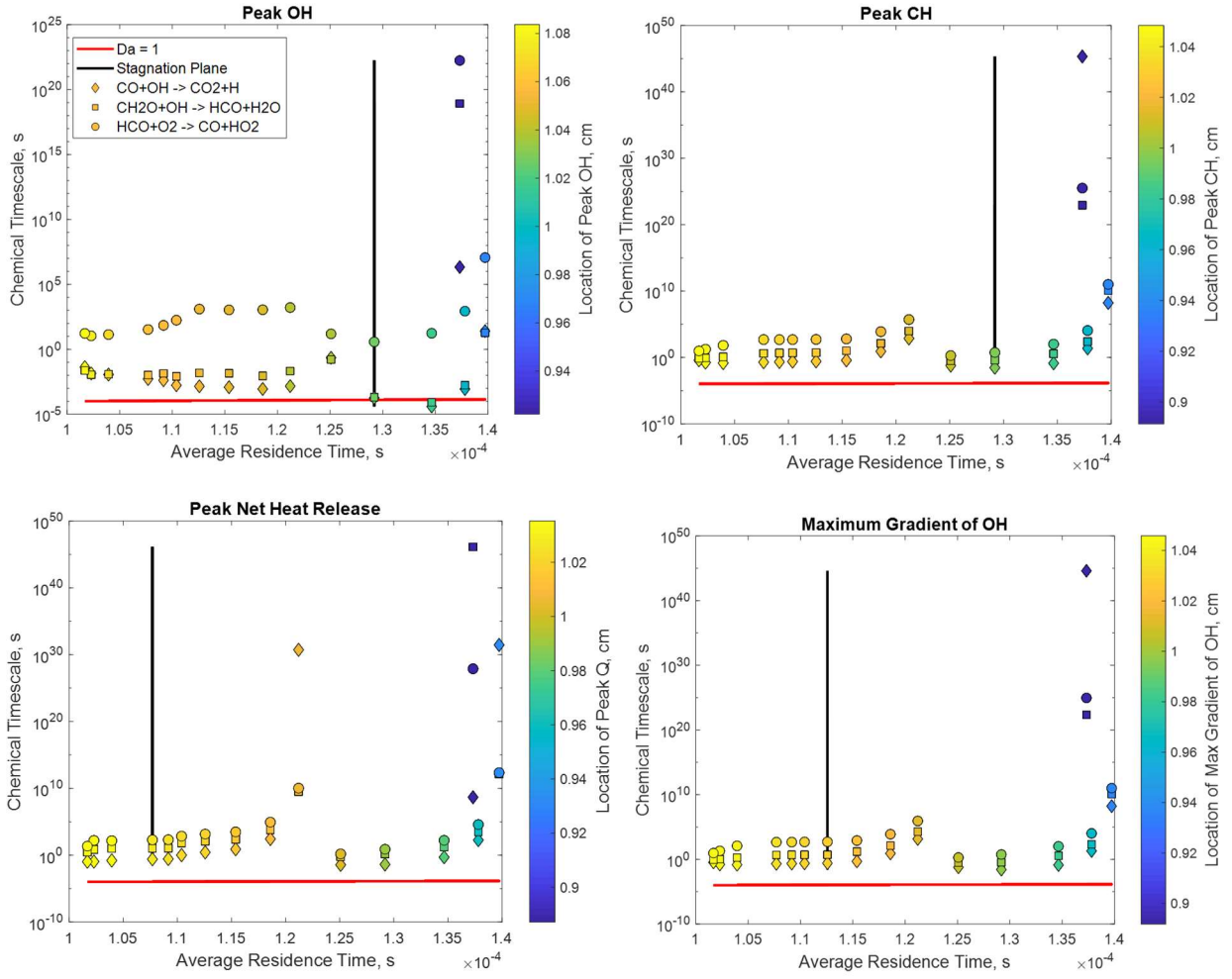

Figure 11. Reaction rates vs. strain residence time with reaction location in the colorbar.

The longest chemical timescale at the peak heat release locations and the maximum gradient of OH locations both occur before the stagnation plan in the premixed reactants region. The maximum gradient of OH is used in LIF to indicate the flame edge and it is unsurprising that those chemical timescales share the same pattern as the peak net heat release location and the peak CH location, as all three are closely linked. If one of the measurement locations is

reporting large reaction rates one would expect the other to since they are so closely linked. One important factor to note is the presence of radicals and key species in the hot product stream. The chemical timescales may be shorter at the higher strain rates because the flame has crossed the stagnation plane and is pumped by the presence of species such as CO, OH, and CO_2 in the hot products stream, indicating the significant differences in flame structure and chemical behavior in a back-supported flame vs. one that is not back-supported.

V. Conclusion

The method of using asymmetric OPPDIF to model premixed turbulent combustion has been used in many previous experiments. In this study, the asymmetric configuration was used to study how the hot products from back-support pilot flames impact the flame structure based on the peak mole fractions of key species and reaction rates of important three important reactions. Additionally, the Chemkin data on reaction rates was combined with experimental data on the residence time of strain to determine if the steady laminar flamelet model was an appropriate way to interpret LIF data.

Based on the data collected from Chemkin on the peak mole fractions, the structure of the flamelet changed at as the strain rates increased. Not only was the peak mole fraction value of key species altered by the increased strain, but the location at which they occurred also changed with the strain. As the strain rate was increased the locations began to shift away from the product stream, towards the stagnation plan and then into the product stream. Additionally, the reaction rates of dominant reactions also changed with the strain. As the strain increased, the reaction rates for $CH_2O + OH \leftrightarrow HCO + H_2O$, $CO + OH \leftrightarrow CO_2 + H$, and $HCO + O_2 \leftrightarrow CO + HO_2$ experience changes. In most cases, the net reaction rates experienced a rapid increase then decrease at lower strain rates followed by a gradual decrease. However, for the $CH_2O + OH \leftrightarrow HCO + H_2O$ reaction, the reaction rate never went to zero even at extremely high strain rates. The reaction rates for $CO + OH \leftrightarrow CO_2 + H$ reversed at the higher strain rates and became negative.

A focus of this study was on the effect of the back-support pilot flames on premixed turbulent combustion experiments. The peak mole fractions from the Chemkin simulations are conflicting as there is a lack of clear extinction even at very high strain rates. The continued reactions at high strains and shift in location to the burned products zone could be attributed to the pool of radicals supplied by the burned products. The burned product temperature combined with the radicals could be enough to create a pseudo preheat zone where the strain rates are too high for a preheat zone to normally exist. This pseudo-preheat zone could be enough to keep the combustion reactions going even at strain rates where extinction should be occurring.

Using a combination of the Chemkin simulations and lab experiments, a diagnostic Damköhler number was created using the reaction rates as the chemical timescale and the average residence time of the strain. Use of this Damköhler number showed that for most strain rates and their corresponding chemical timescales, the residence time at that strain rate was much shorter than the chemical timescale, indicating that the steady laminar flamelet concept is not acceptable for use in modeling these flames. Using this number, only one strain rate at one measurement location was found to have a chemical timescale that was faster than the residence time of the strain. At a jet velocity of 6 m/s and a bulk strain of about 857 s^{-1} the chemical timescale for $CH_2O + OH \leftrightarrow HCO + H_2O$ and $CO + OH \leftrightarrow CO_2 + H$ at the peak OH measurement location outpaced the residence time of the strain. These results have significant implications for the interpretation of multi-species LIF studies to estimate reaction rates.

Acknowledgments

This work was funded by the Air Force Office of Scientific Research under Grant FA9550-16-1-0075 with program monitor Dr. Chiping Li.

References

[1] N. Peters, *Turbulent Combustion*. Cambridge: Cambridge University Press, 2000.

[2] Z. S. Li, B. Li, Z. W. Sun, X. S. Bai, and M. Aldén, "Turbulence and combustion interaction: High resolution local flame front structure visualization using simultaneous single-shot PLIF imaging of CH, OH, and CH2O in a piloted premixed jet flame," *Combust. Flame*, vol. 157, no. 6, pp. 1087–1096, 2010.

[3] M. S. Mansour, N. Peters, and Y.-C. Chen, "Investigation of scalar mixing in the thin reaction zones regime using a simultaneous CH-LIF/Rayleigh laser technique," *Symp. Combust.*, vol. 27, no. 1, pp. 767–773, Jan. 1998.

[4] B. Zhou *et al.*, "Distributed reactions in highly turbulent premixed methane/air flames. Part I. Flame structure characterization," *Combust. Flame*, vol. 162, no. 7, pp. 2937–2953, Jul. 2015.

[5] Z. Wang *et al.*, "Structure and burning velocity of turbulent premixed methane/air jet flames in thin-reaction zone and distributed reaction zone regimes," *Proc. Combust. Inst.*, vol. 37, no. 2, pp. 2537–2544, 2019.

[6] T. M. Wabel, A. W. Skiba, J. E. Temme, and J. F. Driscoll, "Measurements to determine the regimes of premixed flames in extreme turbulence," *Proc. Combust. Inst.*, vol. 36, no. 2, pp. 1809–1816, 2017.
[7] R. Sankaran, E. R. Hawkes, J. H. Chen, T. Lu, and C. K. Law, "Structure of a spatially developing turbulent lean methane-air Bunsen flame," *Proc. Combust. Inst.*, vol. 31 I, no. 1, pp. 1291–1298, 2007.
[8] A. W. Skiba, T. M. Wabel, C. D. D. Carter, S. D. Hammack, J. E. Temme, and J. F. Driscoll, "Premixed flames subjected to extreme levels of turbulence part I: Flame structure and a new measured regime diagram," *Combust. Flame*, vol. 189, pp. 407–432, Mar. 2018.
[9] D. Dasgupta, W. Sun, M. S. Day, and T. C. Lieuwen, "Turbulence effects on the chemical pathways for premixed Methane/Air flames," in *55th AIAA Aerospace Sciences Meeting*, Reston, Virginia: American Institute of Aeronautics and Astronautics, 2017.
[10] G. Coppola, B. Coriton, and A. Gomez, "Highly turbulent counterflow flames: A laboratory scale benchmark for practical systems," *Combust. Flame*, vol. 156, no. 9, pp. 1834–1843, Sep. 2009.
[11] E. Mastorakos, A. M. K. P. Taylor, and J. H. Whitelaw, "Extinction of turbulent counterflow flames with reactants diluted by hot products," *Combust. Flame*, vol. 102, no. 1–2, pp. 101–114, Jul. 1995.
[12] B. Coriton, J. H. Frank, and A. Gomez, "Effects of strain rate, turbulence, reactant stoichiometry and heat losses on the interaction of turbulent premixed flames with stoichiometric counterflowing combustion products," *Combust. Flame*, vol. 160, no. 11, pp. 2442–2456, Nov. 2013.
[13] B. Coriton, J. H. Frank, and A. Gomez, "Interaction of turbulent premixed flames with combustion products: Role of stoichiometry," *Combust. Flame*, vol. 170, pp. 37–52, Aug. 2016.
[14] R. J. Kee, J. A. Miller, G. H. Evans, and G. Dixon-Lewis, "A computational model of the structure and extinction of strained, opposed flow, premixed methane-air flames," *Symp. Combust.*, vol. 22, no. 1, pp. 1479–1494, Jan. 1989.
[15] B. Coriton, M. D. Smooke, and A. Gomez, "Effect of the composition of the hot product stream in the quasi-steady extinction of strained premixed flames," *Combust. Flame*, vol. 157, no. 11, pp. 2155–2164, Nov. 2010.
[16] N. Peters, "Laminar flamelet concepts in turbulent combustion," *Symp. Combust.*, 1988.
[17] H. G. Im, J. H. Chen, and J.-Y. Chen, "Chemical response of methane/air diffusion flames to unsteady strain rate," *Combust. Flame*, vol. 118, no. 1, pp. 204–212, 1999.
[18] A. Tyagi, I. Boxx, S. Peluso, and J. O'Connor, "Statistics and topology of local flame–flame interactions in turbulent flames," *Combust. Flame*, vol. 203, pp. 92–104, 2019.
[19] G. P. Smith *et al.*, "GRI-Mech 3.0," 2019. [Online]. Available: http://www.me.berkeley.edu/gri_mech/.
[20] T. M. Wabel, A. W. Skiba, and J. F. Driscoll, "Evolution of turbulence through a broadened preheat zone in a premixed piloted Bunsen flame from conditionally-averaged velocity measurements," *Combust. Flame*, vol. 188, pp. 13–27, Feb. 2018.
[21] B. Coriton and J. H. Frank, "High-speed tomographic PIV measurements of strain rate intermittency and clustering in turbulent partially-premixed jet flames," *Proc. Combust. Inst.*, vol. 35, pp. 1243–1250, 2015.